# A naphthalene exciplex based Al 3+ selective on-type fluorescent probe for living cells at the physiological pH range: Experimental and computational studies

**ARTICLE** *in* THE ANALYST · MARCH 2012

Impact Factor: 4.11 · DOI: 10.1039/c2an16233d · Source: PubMed



**9 AUTHORS**, INCLUDING:

Animesh Sahana
Nistarini Womens College, SKV University
**52** PUBLICATIONS **747** CITATIONS
SEE PROFILE

Subarna Guha
Central Institute of Plastics Engineering an…
**18** PUBLICATIONS **348** CITATIONS
SEE PROFILE

Bidisha Sarkar
**13** PUBLICATIONS **253** CITATIONS
SEE PROFILE

Debasis Das
University of Burdwan
**137** PUBLICATIONS **1,923** CITATIONS
SEE PROFILE

Analyst

Cite this: *Analyst*, 2012, **137**, 2166

www.rsc.org/analyst

**PAPER**

# A naphthalene exciplex based $Al^{3+}$ selective on-type fluorescent probe for living cells at the physiological pH range: experimental and computational studies†

**Arnab Banerjee,[a] Animesh Sahana,[a] Sudipta Das,[a] Sisir Lohar,[a] Subarna Guha,[a] Bidisha Sarkar,[b] Subhra Kanti Mukhopadhyay,[b] Asok K. Mukherjee*[a] and Debasis Das*[a]**

***Received 8th December 2011, Accepted 25th January 2012***
**DOI: 10.1039/c2an16233d**



2-((Naphthalen-6-yl)methylthio)ethanol (**HL**) was prepared by one pot synthesis using 2-mercaptoethanol and 2-bromomethylnaphthalene. It was found to be a highly selective fluorescent sensor for $Al^{3+}$ in the physiological pH (pH 7.0–8.0). It could sense $Al^{3+}$ bound to cells through fluorescence microscopy. Metal ions like $Mn^{2+}$, $Fe^{3+}$, $Co^{2+}$, $Ni^{2+}$, $Cu^{2+}$, $Zn^{2+}$, $Ag^{+}$, $Cd^{2+}$, $Hg^{2+}$, $Cr^{3+}$ and $Pb^{2+}$ did not interfere. No interference was also observed with anions like $Cl^{-}$, $Br^{-}$, $F^{-}$, $SO_4^{2-}$, $NO_3^{-}$, $CO_3^{2-}$, $HPO_4^{2-}$ and $SCN^{-}$. Experimentally observed structural and spectroscopic features of **HL** and its $Al^{3+}$ complex have been substantiated by computational calculations using density functional theory (DFT) and time dependent density functional theory (TDDFT).

## Introduction

Natural abundance of aluminium in the biosphere is around 8% of the total mineral components. Compounds of aluminium are widely dispersed in the environment in various ways, namely, from water treatment plants, food additives, medicines, anti-perspirants, deodorants, aluminium cookware, cans, bleached flour, antacids, production of light alloys, *etc.* Although aluminium is a non-essential element for living systems, the size (0.051 nm) and charge of $Al^{3+}$ make it a competitive inhibitor of several essential elements of similar characteristics like $Mg^{2+}$ (0.066 nm), $Ca^{2+}$ (0.099 nm) and $Fe^{3+}$ (0.064 nm). It causes dialysis dementia in patients who are unable to eliminate $Al^{3+}$ because of renal dysfunction and also affects the central nervous system to cause different diseases like amyotrophic lateral sclerosis.[1–5] Besides, aluminium toxicity causes microcytic hypochromic anemia, Al-related bone disease (ARBD), and encephalopathy and also has the potential to produce some neurobehavioral and neuro-pathologic changes that are similar to those found in Alzheimer's disease.[6] Apart from these, aluminium toxicity in plant systems is a grave concern, particularly in acidic soil (soil having pH below 5.0), in which phytotoxic $Al^{3+}$ predominates.[7] Generally, it interferes with cell division in root tips and lateral roots, increases cell wall rigidity by cross-linking pectins, reduces DNA replication by increasing the rigidity of DNA double helix, fixes phosphorus in a less available form in soil and root surfaces, decreases root respiration, interferes with enzyme activity governing sugar phosphorylation, deposition of cell wall polysaccharide and the uptake, transport and use of several essential nutrients (Ca, Mg, K, P and Fe).[8] According to a WHO report, the average daily human intake of aluminium is approx. 3–10 mg. The tolerable weekly aluminium intake in the human body is estimated to be 7 mg $kg^{-1}$ of body weight.[9] Therefore, the methods to detect chelatable aluminium ($Al^{3+}$) in biological studies have attracted much attention in recent times. Fluorescent probes for real-time sensing of biologically important ions and fluorescence imaging have become indispensable tools in numerous fields of modern medicine and science.[10] The fluorescence technique offers significant advantages over other methods for metal ion monitoring inside living cells because of its nondestructive character, high sensitivity, instantaneous response, and the availability of a wide range of indicator dyes.[11] Detection of $Al^{3+}$ has always been problematic due to the lack of spectroscopic characteristics and poor coordination ability compared to transition metals.[12] Very few $Al^{3+}$ selective fluorescence sensors have so far been reported,[13] and the majority of them require a tedious synthetic methodology and have poor water solubility.[14] Moreover, if a fluorescent chemosensor with low fluorescence intensity (off-type) shows marked enhancement in fluorescence intensity (on-type) in the presence of $Al^{3+}$, it will be very sensitive for the detection of $Al^{3+}$ in living cells. Thus, there is a great demand for the design and easy synthesis of simple, water soluble and inexpensive $Al^{3+}$ selective on-type fluorescent sensors. Because of the short fluorescence

[a]*Department of Chemistry, The University of Burdwan, Burdwan 713104, India. E-mail: ddas100in@yahoo.com; Fax: +91-342-2530452; Tel: +91-342-2533913*
[b]*Department of Microbiology, The University of Burdwan, Burdwan 713104, India*

† Electronic supplementary information (ESI) available: $^1H$ NMR, QTOF-MS $ES^+$, FTIR, UV-vis, Job's plot, theoretical IR spectrum, and tables of natural population analysis of **HL** and its $Al^{3+}$ complex. See DOI: 10.1039/c2an16233d

lifetime,[15] low fluorescence quantum yield[16] and ability to act as a donor as well as an acceptor,[17] naphthalene can be chosen as an ideal component of a fluorescent chemosensor. Easy coupling of the naphthalene moiety to a hydrophilic tail enhances its water solubility and makes it suitable for monitoring $Al^{3+}$ in living cells. The present report is aimed to achieve these objectives.

## Experimental

### General procedures

High-purity HEPES and 2-bromomethylnaphthalene were purchased from Sigma Aldrich (India). 2-Mercaptoethanol was purchased from Alfa Aesar (Germany). $Al(NO_3)_3 \cdot 9H_2O$ was purchased from Merck (India). Spectroscopic grade solvents were used. Other chemicals were of analytical reagent grade and were used without further purification except when specified. Milli-Q 18.2 MΩ $cm^{-1}$ water was used throughout the experiments. A JASCO (model V-570) UV-vis spectrophotometer was used for measuring the UV-vis spectra. FTIR spectra were recorded on a JASCO FTIR spectrometer (model: FTIR-H20). Mass spectra were measured using a QTOF Micro YA 263 mass spectrometer in ES positive mode. $^1H$ NMR spectra were recorded using Bruker Avance 600 (600 MHz) and Bruker Advance 200 (200 MHz) spectrometers in DMSO-$d_6$ and $CDCl_3$. Elemental analysis was performed using a Perkin Elmer CHN-Analyser with first 2000-Analysis kit. Steady-state fluorescence experiments were performed using a Hitachi F-4500 spectrofluorimeter equipped with a temperature controlled cell holder. pH measurements were carried out on a Systronics digital pH meter (model 335, India). All spectra were recorded at room temperature except for fluorescence microscope images.

Structures of **HL** and its $Al^{3+}$ complex were optimized by DFT and TDDFT using the Gaussian 03 software package.[18]

### Imaging system

The imaging system was comprised of an inverted fluorescence microscope (Leica DM 1000 LED), a digital compact camera (Leica DFC 420C), and an image processor (Leica Application Suite v3.3.0). The microscope was equipped with a mercury 50 W lamp.

### Preparation of cells

To detect intracellular $Al^{3+}$, *Candida albicans* cells (IMTECH no. 3018) from exponentially growing culture in yeast extract glucose broth medium (pH 6.0; incubation temperature, 37 °C) were centrifuged at 3000 rpm for 10 minutes and washed twice with 0.1 M HEPES buffer at pH 7.4. Then, they were treated with 20 μM $Al^{3+}$ salt for 30 minutes in 0.1 M HEPES buffer (pH 7.4) containing 0.01% Triton X100 as a permeability enhancing agent. After incubation the cells were washed again with HEPES buffer at pH 7.4 and incubated with **HL** (10 μM) for 15 minutes. **HL** treated cells were mounted on a grease free glass slide and observed under a Leica DM 1000 fluorescence microscope equipped with a UV filter. Cells without $Al^{3+}$ treatment but incubated with ligand were used as control.

### Synthesis of 2-((naphthalen-6-yl)methylthio)ethanol (HL) (Scheme 1)

104 mg (4.52 mmol) Na was put in 10 mL dry EtOH under nitrogen atmosphere (at 0 °C) with constant stirring until complete dissolution. Then, 5 mL solution of 2-mercaptoethanol (353.14 mg, 4.52 mmol) in dry EtOH was added under stirring conditions for half an hour followed by the addition of 1 g (4.52 mmol) of 2-bromomethylnaphthalene. Stirring was continued for additional two hours. After rotary evaporation of the solvent, the crude product was subjected to column chromatography (hexane : EtOAc = 81 : 19). Yield 65%; mp 52 °C (±4 °C); $^1H$ NMR (600 MHz, DMSO-$d_6$) (Fig. S1 in ESI†): $\delta$ (ppm): 2.4 (2H, t, $J$ = 6.6 Hz), 3.5 (2H, q, $J$ = 6.6 Hz), 3.9 (2H, s), 4.7 (1H, t, $J$ = 5.4 Hz), 7.466–7.516 (3H, m, $J$ = 6.0 Hz), 7.789 (1H, S), 7.859–7.889 (3H, m, $J$ = 6 Hz); $^{13}C$ NMR (600 MHz, DMSO-$d_6$) (Fig. S2 in ESI†): $\delta$ (ppm): 136.39, 132.82, 132.00, 128.05, 127.56, 127.51, 127.01, 126.23, 125.77, 60.63, 35.51, 33.27; QTOF-MS $ES^+$: $[M + Na]^+$ (Fig. S3 in ESI†) = 241.08 (100%); elemental analysis data as calculated for $C_{13}H_{14}OS$ (%): C, 71.52; H, 6.46. Found (%): C, 71.28; H, 6.72. FTIR ($cm^{-1}$): (Fig. S4 in ESI†) $\nu$(OH) 3339.3.

### Synthesis of $[Al(L)(HL)(NO_3)_2(H_2O)(CH_3OH)]$

Methanol solution of $Al(NO_3)_3 \cdot 9H_2O$ (0.172 g, 0.45 mmol, 10 mL) was added slowly to a solution of **HL** (0.2 g, 0.91 mmol, 10 mL) in methanol under stirring conditions and continued for 15 minutes. Then the mixture was refluxed for 15 minutes to get a clear solution which on keeping overnight yielded an off-white colored compound. Yield: 75%. $^1H$ NMR (200 MHz, $CDCl_3$) (Fig. S5 in ESI†), $\delta$ (ppm): 1.8 (3H), 2.5 (4H), 3.5 (4H), 3.8 (4H), 6.4 (4H), 7.3 (6H), 7.6 (8H). QTOF-MS $ES^+$ (Fig. S6 in ESI†): $[M + Na]^+$ = 659.22. FTIR ($cm^{-1}$) (Fig. S4 in ESI†): $\nu$(OH) 3405.6; $\nu(NO_3^-)$ 1384.6, 1042.3.

## Results and discussion

### Absorption studies

The UV-vis absorption spectra of **HL** (2-((naphthalen-6-yl) methylthio)ethanol) and its isolated $Al^{3+}$ complex in aqueous ethanol (9.5/0.5, v/v) solution ($10^{-4}$ M) are shown in Fig. S7 (ESI†) where a broad absorption band in the range 330–450 nm was observed. The absorption spectrum of **HL** exhibited a maximum absorption at 225 nm with shoulders at 265, 275 and 287 nm. Spectral changes of the system upon gradual addition of

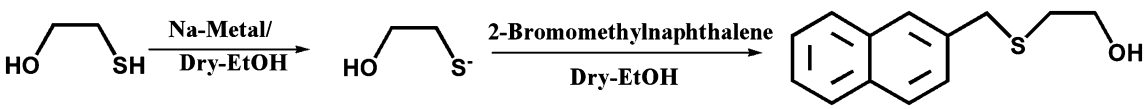


Scheme 1

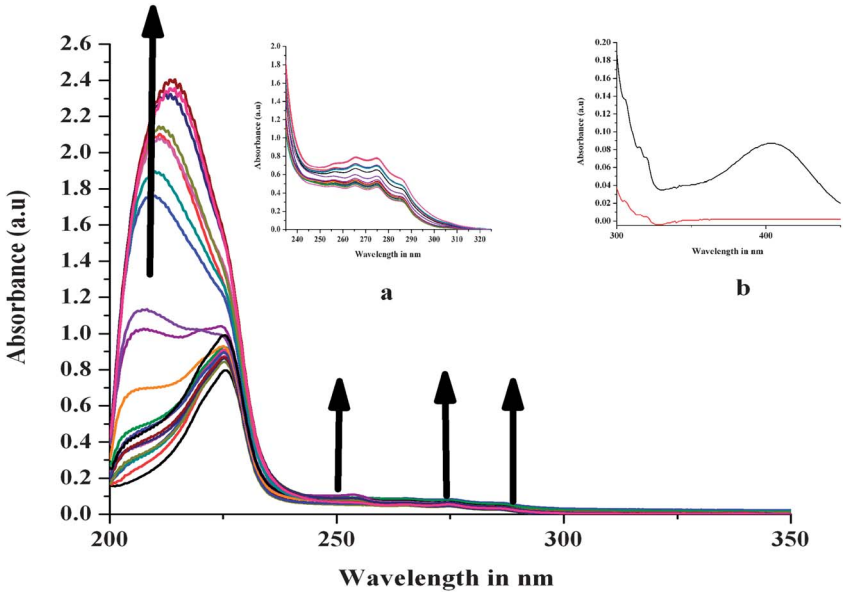


**Fig. 1** Changes in the absorption spectra of **HL** (10 μM) as a function of added $Al^{3+}$ (1–50 μM) in methanol at room temperature. Inset: (a) **HL** (100 μM) + $Al^{3+}$ (10–500 μM) and (b) **HL** (1000 μM) + $Al^{3+}$ (2000 μM), **HL** (red) and ligand + $Al^{3+}$ system (black).

$Al^{3+}$ (1–50 μM; inset (a) 10–500 μM) are shown in Fig. 1. It was found that a low-intensity broad tail gradually developed in the range 330–450 nm and the $\lambda_{max}$ of **HL** was prominently blue-shifted and intensified.

### Emission studies

Upon excitation of **HL** at 350 nm (at pH 7.4, 50 mM HEPES buffer), the emission spectrum of **HL** showed the maximum intensity at 449 nm with a low quantum yield value of 0.013 (details are shown in the ESI†). This is attributed to the emission of the exciplex formed between excited naphthalene and lone pair electrons on the $–CH_2–$ bridged S atom. Formation of such exciplex emitting at 449 nm was reported earlier.[19] The low intensity of this 449 nm band in the present study is due to quenching by the –OH receptor through a PET (photoinduced electron transfer) mechanism.[20] The 449 nm emission intensity of **HL** (1.0 μM) increased gradually on addition of $Al^{3+}$ (0.1–5 μM) and the fluorescence quantum yield of the system increased more than 6-fold to a value of 0.083. The reason for such a large fluorescence enhancement might be attributed to the decrease of PET in the presence of $Al^{3+}$ ions (Fig. 2). This observation was also corroborated by computational studies in terms of charge distribution on the fluorophore upon complexation with $Al^{3+}$. The changes in the fluorescence emission intensities of **HL** (1 μM) as a function of added $Al^{3+}$ concentration are presented in Fig. 3.

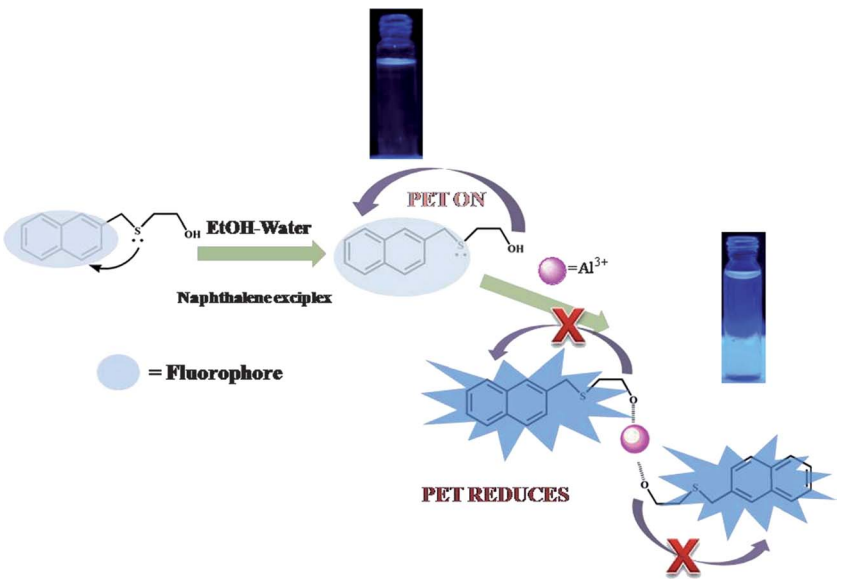


**Fig. 2** Schematic fluorescence enhancement mechanism of **HL** in the presence of $Al^{3+}$.

 

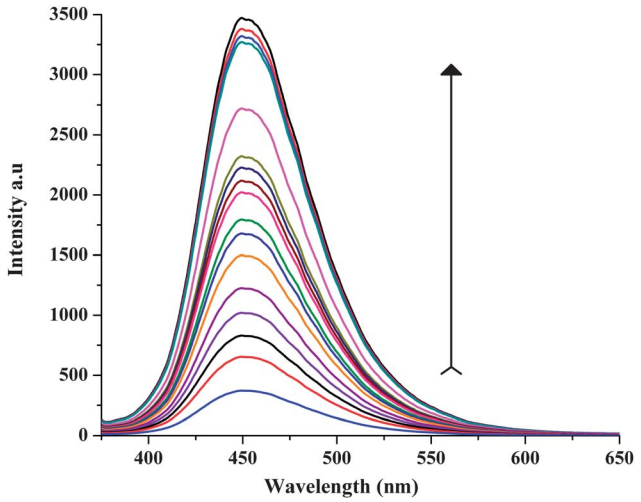


**Fig. 3** Emission spectra of **HL** (1.0 μM) in the presence of 0.1 to 5.0 μM solution of $Al^{3+}$ in 50 mM HEPES buffer at pH 7.4 at room temperature ($\lambda_{em}$: 449 nm, $\lambda_{ex}$: 350 nm).

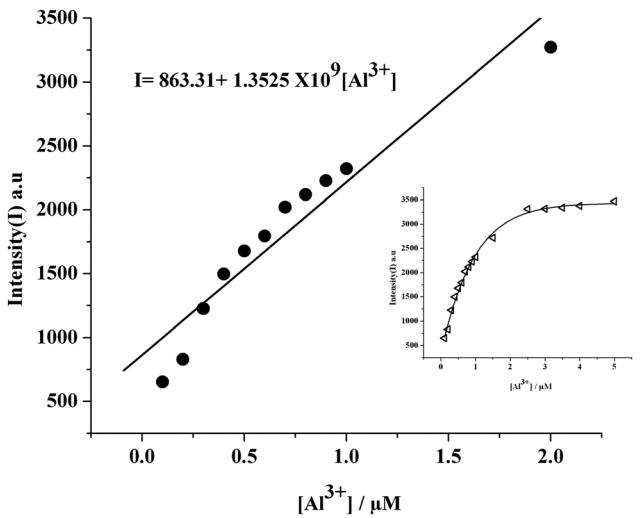


**Fig. 4** Plot of emission intensities *vs.* $[Al^{3+}]$ ([**HL**] = 1 μM, $[Al^{3+}]$ = 0.1–2.0 μM). Inset: [**HL**] = 1 μM, $[Al^{3+}]$ = 0.1–5.0 μM ($R^2$ = 0.97).

The plot of emission intensity as a function of externally added $[Al^{3+}]$ (Fig. 4) revealed that above a certain amount of externally added $[Al^{3+}]$, there was no further change in the emission intensity of the system (inset of Fig. 4). Up to 2 μM of the externally added $[Al^{3+}]$, the plot was linear. From this linear relationship (Fig. 4), one could easily determine the concentration of unknown $Al^{3+}$ in aqueous solution. The detection limit of the ligand is $1 \times 10^{-8}$ M in aqueous ethanol (95/05, v/v) solution. A significant point to be mentioned here is that the fluorophore of the sensor is not the naphthalene itself, but an exciplex of the naphthalene –$CH_2$–S– moiety whose emission is quenched by the receptor –OH by PET. Due to its size and charge, $Al^{3+}$ interacted only with the O atom which reduced the PET and enhanced the fluorescence intensity. Except $Al^{3+}$, several other metal ions in the present study interact with the S-atom which break the exciplex of the naphthalene –$CH_2$–S– moiety and quench the fluorescence intensity. Thus no significant enhancement of fluorescence

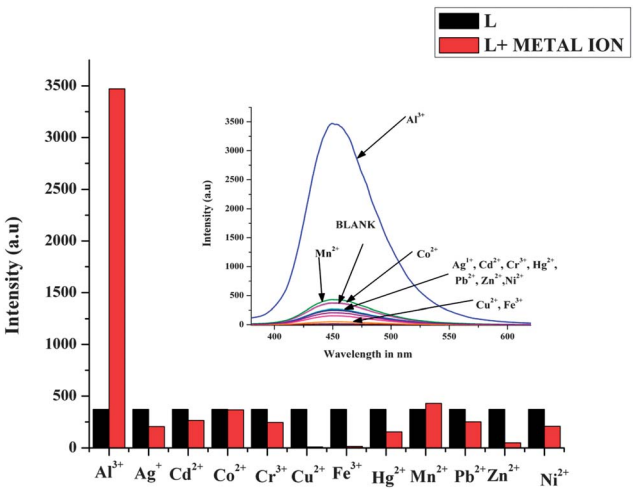


**Fig. 5** Effect of foreign ions (50 μM) on the emission intensities of **HL** (10 μM).

intensity of **HL** was observed upon addition of the equivalent amount of metal ions like $Mn^{2+}$, $Fe^{3+}$, $Co^{2+}$, $Ni^{2+}$, $Cu^{2+}$, $Zn^{2+}$, $Ag^{+}$, $Cd^{2+}$, $Hg^{2+}$, $Cr^{3+}$ and $Pb^{2+}$ (Fig. 5).

It was well known that performance of fluorescence sensors based on the electron donor/acceptor mechanism depends largely on the concentration of proton in the medium as it competed with the metal ion of interest for binding the ligand. Thus, optimization of pH on the efficiency of the sensor was essential. Fluorescence pH titrations were carried out for this purpose in aqueous ethanol (95/05, v/v) solution. Equivalent amounts of **HL** and $Al^{3+}$ were taken in different sets of pH (pH 1.5–12.0). Fig. 6 clearly demonstrates that from pH 7.0 to 8.0, the **L**–$Al^{3+}$ system showed maximum emission intensity. Fluorescence emission intensity of **HL** remained unchanged on addition of $Al^{3+}$ at pH below 6.9 and above 8.0. Most plausibly, protonation of **L** at pH below 6.9 inhibited it to coordinate $Al^{3+}$. Over pH 8.0, competition of $OH^{-}$ with **L** for binding $Al^{3+}$ succeeded.

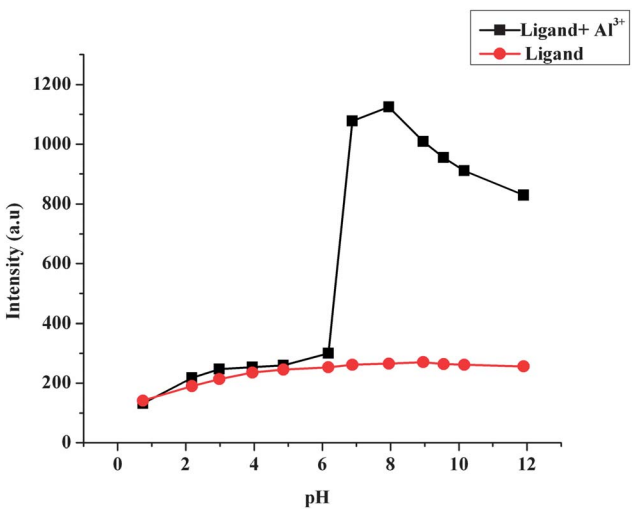


**Fig. 6** Effect of pH on the binding efficiency of **HL** (10 μM) towards $Al^{3+}$ (10 μM) ($\lambda_{em}$: 449 nm, $\lambda_{ex}$: 350 nm).

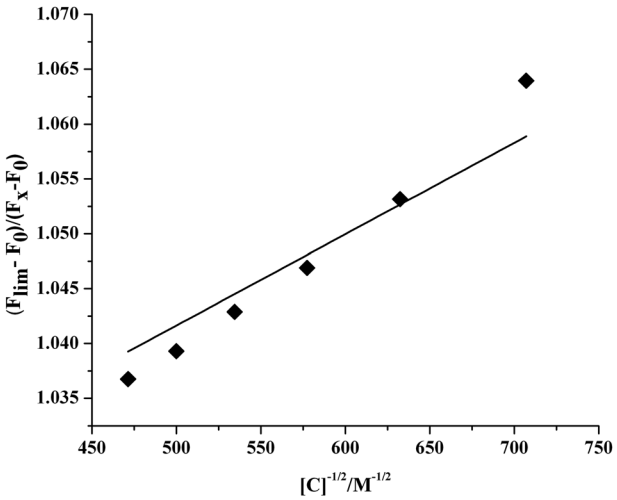


**Fig. 7** Determination of the binding constant ($K_a$) of **L** for $Al^{3+}$ ($2.0 \pm 0.3$) $\times$ $10^4$ $M^{-1/2}$ ($R^2 = 0.95$).

## Binding studies

Job's plot indicated a 2 : 1 stoichiometry of the complex formed between ligand and $Al^{3+}$ (Fig. S8 in ESI†), which was also corroborated from the mass spectra of the $Al^{3+}$ complex. To study the binding interaction of ligand with $Al^{3+}$ in buffer medium, the binding constant value had been estimated from the emission intensity data following the modified Benesi–Hildebrand equation:[21]

$$(1/\Delta F) = 1/\Delta F_{max} + (1/K[C]^n)(1/\Delta F_{max}).$$

Here $\Delta F = (F_x - F_0)$ and $\Delta F_{max} = F_\infty - F_0$, where $F_0$, $F_x$, and $F_\infty$ are the emission intensities of ligand in the absence of $Al^{3+}$, at an intermediate $Al^{3+}$ concentration, and at a concentration of complete interaction, respectively. While $K$ is the binding constant, $[C]$ represents the concentration of $Al^{3+}$ and $n$ is the number of $Al^{3+}$ bound per ligand (in our case, $n = 0.5$). From the plot of $(F_\infty - F_0)/(F_x - F_0)$ against $[C]^{-1/2}$ (Fig. 7), the value of $K$ was extracted from the slope as $2.0 \times 10^4$ $M^{-1/2}$.

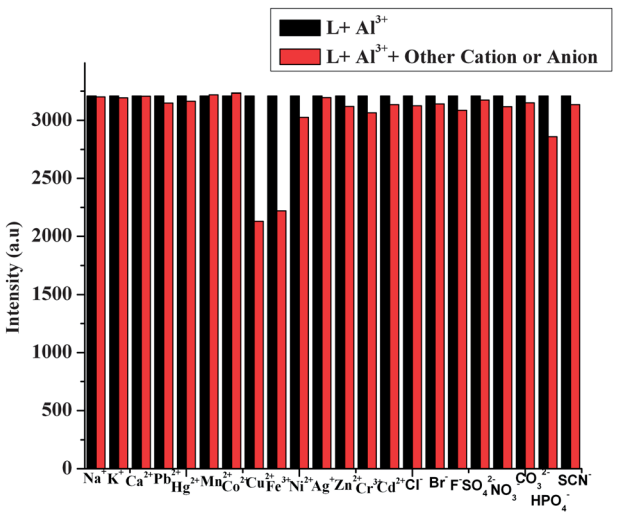


**Fig. 8** Interferences of foreign ions (20 μM) in the emission intensities of **HL** (10 μM) in the presence of $Al^{3+}$ (20 μM) in HEPES buffer (water : ethanol = 95/5, v/v, pH 7.4).

Fig. 8 shows the fluorescence response of **HL** to $Al^{3+}$ in the presence of equivalent amounts of alkali, alkaline earth, transition metal ions and a good number of anions in HEPES buffer solution (water : ethanol = 95/5, v/v, pH 7.4). A minor quenching effect of Fe(III) and Cu(II) did not cause any harm to the determination of $Al^{3+}$.

The hexa-coordination of $Al^{3+}$ has been satisfied by two ligands (one **HL** and the other is **L** form), two nitrate groups, one methanol and one water molecule. This was supported by mass spectra, elemental analysis, $^1$H NMR spectra and FTIR spectra. Non-polar (neutral) nature of the complex also supported this composition.

Fluorescence studies were carried out in aqueous ethanol (95/05, v/v) solution where a rapid reversible equilibrium could exist as shown below. Thus, free $Al^{3+}$ was always available for the

$$Al^{3+} + n(\text{solvent}) \rightleftharpoons [Al(\text{solvent})_n]^{3+}$$

ligand to form the complex. This fact could be supported by the fact that although the composition of the $Al^{3+}$ complex had been established as 2 : 1 (ligand: $Al^{3+}$, from Job's plot, mass spectra, *etc.*), yet in the fluorescent titration experiment saturation point was achieved only after the addition of 5 equivalents of $Al^{3+}$ ion which shifted the equilibrium to the product side to the maximum extent.

It is worth mentioning here that although under ESI conditions, the molecule could break into fragments, but there is probability, however low, that some molecules remain unbroken, which are responsible for the low intensity molecular ion peak in all types of mass spectrometry.[13] In the present case also, we have observed a low intensity peak at $m/z = 659.22$ for the complex–$Na^+$ adduct with adequate number of satellite peaks due to the presence of S-atom.

To establish and justify the fact that it is the $Al^{3+}$ and not the nitrate ion which was responsible for the fluorescence enhancement of the ligand, two facts were presented: (i) $Al_2(SO_4)_3$ has also enhanced the fluorescence intensity of the ligand and (ii) nitrate assisted oxidation of the sulfide group of the probe to the sulfoxide was ruled out from the fact that the red–ox potential value of $NO_3^-/N_2$ in acid medium is 1.25 V and in basic medium is 0.25 V. So, if the fluorescence enhancement would occur due to oxidation, then the best result would have been observed in the acid medium. But a pH study had shown that the maximum enhancement of emission intensity of the $Al^{3+}$ complex was observed in the basic range.

## NMR titration

NMR spectroscopy has been used to ascertain the binding mode of the ligand to $Al^{3+}$. Mass and FTIR spectra of the isolated $Al^{3+}$ complex (ESI†) revealed that in the solid state both **L** and **HL** forms of the ligand bind to $Al^{3+}$. $^1$H NMR spectra of the isolated $Al^{3+}$ complex in $CDCl_3$ solution had also indicated **L/HL** combination of the complex. To study the binding interaction of the ligand with $Al^{3+}$ in solution, $^1$H NMR spectra of **HL** were recorded in DMSO-$d_6$ upon gradual addition of varying concentrations of $Al^{3+}$. Significant spectral changes were

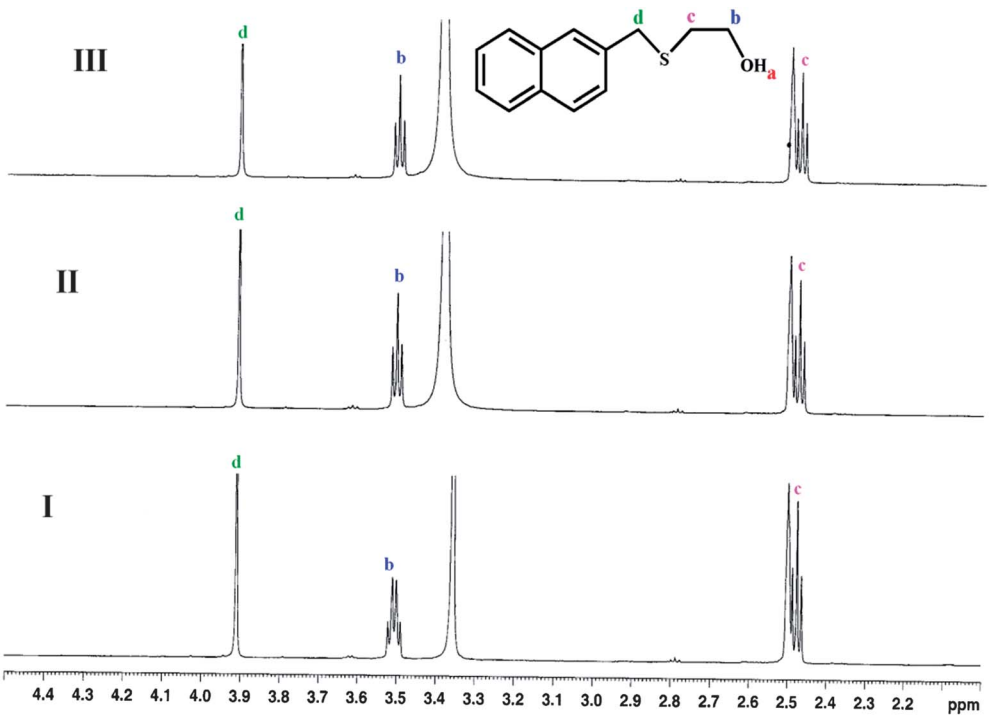


**Fig. 9** Changes in the $^1$H NMR spectra of **HL** upon addition of $Al^{3+}$ in DMSO-$d_6$: (I) only **HL**, (II) **HL** with 1 equivalent $Al^{3+}$ and (III) **HL** with 2.0 equivalents $Al^{3+}$.

**Table 1** Changes in chemical shift of different protons in NMR titration

| | OH (a) | O–$CH_2$ (b) | | S–$CH_2$ (c) | | Ar–$CH_2$ (d) | |
|---|---|---|---|---|---|---|---|
| | $\delta$ (ppm) | $\delta$ (ppm) | Change in $\delta$ | $\delta$ (ppm) | Change in $\delta$ | $\delta$ (ppm) | Change in $\delta$ |
| **HL** | 4.790–4.772, triplet | 3.522–3.490, quartet | | 2.488–2.465, triplet | | 3.911, singlet | |
| **HL** + $Al^{3+}$ (1 : 1) | — | 3.505–3.478, triplet | 0.012 (up-field) | 2.487–2.464, triplet | 0.001 (up-field) | 3.909, singlet | 0.002 (up-field) |
| **HL** + $Al^{3+}$ (1 : 2) | — | 3.504–3.476, triplet | 0.014 (up-field) | 2.486–2.463, triplet | 0.002 (up-field) | 3.907, singlet | 0.004 (up-field) |

observed as shown in Fig. 9. Upon addition of $Al^{3+}$, the $\delta$ 4.7 signal for free –OH disappeared and the O–$CH_2$ signal ($\delta$ 3.49, quartet) of the free ligand became a triplet with a slight up-field shift. Although the extent of chemical shifts was small (Table 1), it was well within the range as observed by other workers[13b,22] for similar types of studies. But no significant change of the S–$CH_2$ and naphthalene–$CH_2$ protons was observed on complexation (Table 1). Deprotonation of **HL** caused by the addition of $Al^{3+}$ to its solution had created a negative charge on the O atom which has resulted in an up-field shift of the proton adjacent to the C atom of the O–$CH_2$ group. When $Al^{3+}$ did bind with the O atom, the negative charge on $O^-$ was withdrawn towards $Al^{3+}$ to some extent, thereby decreasing the electron density on the O–$CH_2$ protons. Thus, complexation induced changes in $\delta$ value may be attributed to the resultant of these two mutually opposing effects. Significant fluorescence enhancement of the ligand in basic medium had also supported the presence of **L** in the $Al^{3+}$ complex. These findings were further substantiated by DFT calculated charge density (natural population analysis) measurement as shown in Table 2.

**Table 2** Comparison between the DFT calculated NPA charges on H atoms of **HL** and **L** bound to $Al^{3+}$

| | **HL** | **L**–$Al^{3+}$ complex |
|---|---|---|
| O–$CH_2$ (b) | 0.20378 | 0.19691 |
| | 0.19980 | 0.18002 |
| S–$CH_2$ (c) | 0.24631 | 0.24682 |
| | 0.23934 | 0.22815 |
| Ar–$CH_2$ (d) | 0.24161 | 0.24822 |
| | 0.24514 | 0.23488 |

## Computational studies

### Structural features

Geometry optimization, frequency calculation, UV-vis spectra analysis and natural population analysis of **HL** were performed using both 6-31++G (d, p) and LANL2DZ (Table 3) basis sets. No significant difference was observed for the two basis sets used. For the $Al^{3+}$ complex, the basis set LANL2DZ was used.

**Table 3** Comparison of selected bond lengths and angles of **HL** using LANL2DZ and 6-31++G (d, p) basis sets

| LANL2DZ | | 6-31++G (d, p) | |
|---|---|---|---|
| Bond lengths/Å | Bond angles/° | Bond lengths/Å | Bond angles/° |
| O(28)–C(25) 1.452 | O(28)–C(25)–C(22) 107.16 | O(28)–C(25) 1.436 | O(28)–C(25)–C(22) 108.63 |
| C(25)–C(22) 1.523 | C(25)–C(22)–S(21) 110.99 | C(25)–C(22) 1.520 | C(25)–C(22)–S(21) 111.63 |
| C(22)–C(21) 1.893 | C(22)–S(21)–C(18) 98.18 | C(22)–C(21) 1.850 | C(22)–S(21)–C(18) 98.72 |
| C(21)–C(18) 1.911 | | C(21)–C(18) 1.961 | |
| C(18)–C(15) 1.508 | | C(18)–C(15) 1.506 | |



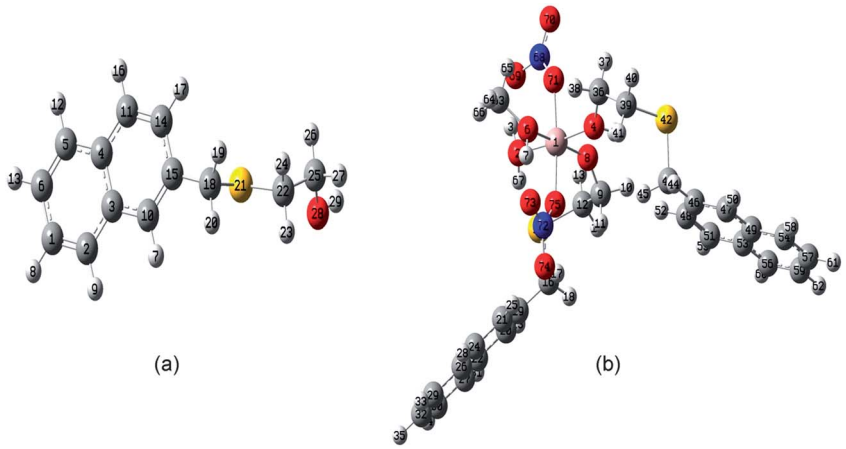


**Fig. 10** Optimized geometry of (a) **HL** and (b) [Al(**L**)(**HL**)$(NO_3)_2(H_2O)(CH_3OH)$].

**Table 4** Relevant bond lengths and angles of the **L**–$Al^{3+}$ complex (atom numbering refers to Fig. 10a and b) using the LANL2DZ basis set

| Bond angles/° | Bond lengths/Å |
|---|---|
| O(4)(**HL**)–Al(1)–O(8)(**L**) 84.62 | Al(1)–O(2)($H_2O$) 1.922 |
| O(4)(**HL**)–Al(1)–O(75)($NO_3^-$) 93.97 | Al(1)–O(4)(**HL**) 1.955 |
| O(4)(**HL**)–Al(1)–O(71)($NO_3^-$) 85.80 | Al(1)–O(6)($CH_3OH$) 1.949 |
| O(4)(**HL**)–Al(1)–O(6)($CH_3OH$) 86.89 | Al(1)–O(8)($L^-$) 1.788 |
| O(4)(**HL**)–Al(1)–O(2)($H_2O$) 175.73 | Al(1)–O(71)($NO_3^-$) 1.966 |
| O(8)(**L**)–Al(1)–O(2)($H_2O$) 97.62 | Al(1)–O(75)($NO_3^-$) 2.025 |
| O(8)(**L**)–Al(1)–O(6)($CH_3OH$) 169.33 | |
| O(8)(**L**)–Al(1)–O(71)($NO_3^-$) 99.07 | |
| O(8)(**L**)–Al(1)–O(75)($NO_3^-$) 88.37 | |
| O(6)($CH_3OH$)–Al(1)–O(75)($NO_3^-$) 85.76 | |
| O(6)($CH_3OH$)–Al(1)–O(71)($NO_3^-$) 86.71 | |
| O(6)($CH_3OH$)–Al(1)–O(2)($H_2O$) 91.26 | |
| O(75)($NO_3^-$)–Al(1)–O(71)($NO_3^-$) 172.48 | |
| O(75)($NO_3^-$)–Al(1)–O(2)($H_2O$) 89.72 | |
| O(71)($NO_3^-$)–Al(1)–O(2)($H_2O$) 90.25 | |

The optimized geometry of **HL** and its $Al^{3+}$ complex is shown in Fig. 10a and b, respectively. For **HL**, the values for energy (RB + HF-LYP), RMS gradient norm and the dipole moment were −977.27361665 a.u., 0.00000476 a.u. and 2.4383 D, respectively. For $Al^{3+}$ complex, the said values were −1932.45877526 a.u., 0.00000916 a.u. and 4.2301 D, respectively. Both **HL** and $Al^{3+}$ complex had C1 point group. Some relevant bond lengths and bond angles around the $Al^{3+}$ ion are given in Table 4. The geometry of the $Al^{3+}$ complex around the $Al^{3+}$ was a slightly distorted octahedron where two nitrate ions were *trans* to each other. **HL** was *trans* to the coordinated $H_2O$ and **L** was *trans* to the coordinated $CH_3OH$. **L** and **HL** were *cis* to each other and solvent molecules, *viz.* $H_2O$ and $CH_3OH$ were also *cis* to each other (Fig. 10). The distance between O(8) of **L** and H(5) of **HL** was 2.2420 Å (H–X angle 119° was also greater than 90° which is favorable for intra-molecular H-bonding), an ideal distance for the formation of intra-molecular H-bonds, leading to an extra stability of the system. Two H atoms of water molecule (3) and (67) took part in the intra-molecular H-bonding with the O atoms of $NO_3^-$(69) and **L** (8) (O to H distances were 1.649 Å and 2.289 Å and the H–X angles were 109° and 94°, respectively) The –OH proton of methanol also formed H-bond with the O atom (73) of the other $NO_3^-$ (O to H distance was 1.5539 Å and H–X

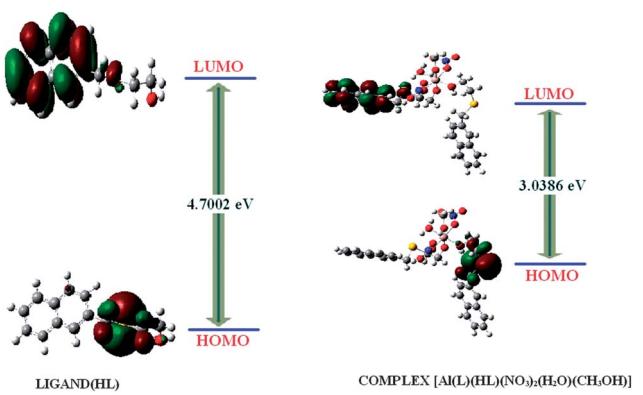


**Fig. 11** HOMO and LUMO of **HL** and [Al(**L**)(**HL**)$(NO_3)_2(H_2O)$-$(CH_3OH)$].

angle was 159°). The Highest Occupied Molecular Orbital (HOMO) and the Lowest Unoccupied Molecular Orbital (LUMO) of the **HL** and its $Al^{3+}$ complex are presented in Fig. 11. The energy gaps between HOMO and LUMO in the ligand and $Al^{3+}$ complex were 4.7002 eV and 3.0386 eV respectively.

### Natural Population Analysis (NPA)

Explanation for fluorescence enhancement was provided as follows: NPA showed (Tables S1 and S2 in ESI†) that the total electronic charge on the fluorophore moiety was 0.17 in the free ligand and 0.62 in the $Al^{3+}$ complex. Also, charges on oxygen were −0.77 and −0.88 in the free ligand and $Al^{3+}$ complex, respectively, which clearly indicated a decrease of the PET process leading to fluorescence enhancement. All the exchangeable –OH protons (**HL**, $H_2O$, and $CH_3OH$) of the complex exhibited $^1H$ NMR signal in the downfield region ($\delta$ 6.4) compared to the non-aromatic protons of the complex (Fig. S5 in ESI†) which could also be explained from the calculated charges (0.5512 − 0.5200) using natural population analysis (Tables S1 and S2 in ESI†).

### IR, UV-vis and NMR spectra

The optimized geometry of the $Al^{3+}$ complex was also used for IR frequency calculation. No imaginary frequency was observed indicating that the optimized geometry corresponded to a real energy minimum and not a saddle point. Experimentally

**Table 5** Theoretical *vs.* experimental IR data of **HL** and its $Al^{3+}$ complex

| | Theoretical, $\nu$/cm$^{-1}$ | Experimental, $\nu$/cm$^{-1}$ |
|---|---|---|
| **HL** | 460, 492, 767, 833, 860, 1085, 1269, 1294, 1333, 1443, 1472, 1517, 2988, 3042, 3097, 3194, 3841 | 476, 487, 745, 831, 864, 1045, 1126, 1146, 1169, 1212, 1233, 1276, 1362, 1425, 2918, 3052, 3339, 3906 |
| **L**–$Al^{3+}$ complex | 383, 434, 498, 613, 719, 790, 872, 932, 985, 1026, 1076, 1282, 1359, 1410, 1451, 1586, 1692, 2926, 3168, 3298, 3579 | 395, 456, 485, 619, 745, 830, 865, 897, 950, 1012, 1042, 1384, 1504, 1636, 3405 |

**Table 6** Theoretical *vs.* experimental UV-vis spectral data of **HL** and its $Al^{3+}$ complex

| | Theoretical, $\lambda$/nm (osc. strength) | Experimental, $\lambda$/nm |
|---|---|---|
| **HL** | 230 (1.2766), 254 (0.0292), 279 (0.0403), 287 (0.0325), 293 (0.0428) | 225 ($\lambda_{max}$), 265, 275, 287 |
| **L**–$Al^{3+}$ complex | 410 (0.0042), 352 (0.0019), 348 (0.0010), 345 (0.0020), 293 (0.0728), 285 (0.0025), 266 (0.0418) | 210, 231, 261, 266, 275, 286 and low-intensity broad hump gradually ranges 330–450 with maxima at 410 |

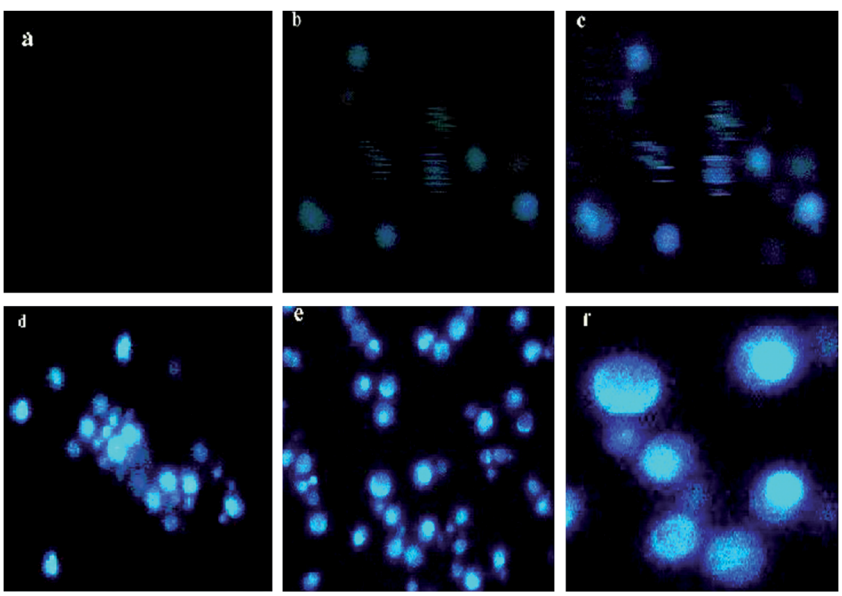


**Fig. 12** Fluorescence microscopic images with 100× objective lens: (a) image of *Candida albicans* in the absence of **HL**, (b) image of **HL** treated *Candida albicans* in the absence of $Al^{3+}$, (c) image of *Candida albicans* after treatment of both **HL** and $Al^{3+}$ in the absence of Triton X100, (d) image of *Candida albicans* after treatment of both **HL** and $Al^{3+}$ in the presence of 0.01% Triton X100 observed after 15 minutes, (e) image of *Candida albicans* after treatment of both **HL** and $Al^{3+}$ in the presence of 0.01% Triton X100 observed after 30 minutes, and (f) enlarged view of (e).

observed (Fig. S4) and theoretically calculated (Fig. S9 and S10) IR spectra are presented in Table 5. UV-vis spectra of **HL** and its $Al^{3+}$ complex were calculated using the TDDFT method in gas phase and methanol. For methanol the CPCM formalism was imposed which had considered the solvent as a polarizable continuum and did not include discrete solvent molecules for solvation of the solute.[23] Calculated absorption peaks had agreed well with the experimentally observed peaks (Table 6). Experimental UV-vis spectra of **HL** and its $Al^{3+}$ complex are presented in Fig. S7 (ESI†). Theoretical UV-vis spectra of **HL** and its $Al^{3+}$ complex are shown in Fig. S11 and S12, respectively (ESI†). The prominent electronic transitions of the ligand and its $Al^{3+}$ complex along with their orbital contributions are presented in Tables S3 and S4 (ESI†), respectively, and their corresponding orbital pictures are shown in Table S5 (ESI†). In the case of the ligand, the transition from HOMO → LUMO contributed mainly to the excitation at 293 nm; whereas transitions from HOMO − 2 → LUMO and HOMO → LUMO + 1 had contributed mainly to the excitation at 230 nm. For the $Al^{3+}$ complex, main absorption peaks in the long wavelength region were at 410 nm, 352 nm and 348 nm. The peak at 410 nm was generated from the transition HOMO − 2 → LUMO; peak at 352 nm was generated from the transition HOMO − 4 → LUMO + 1 and peak at 348 nm was generated from the transition HOMO − 6 → LUMO + 1. Gas phase NMR spectra of **HL** and its $Al^{3+}$ complex were theoretically calculated using GIAO, CSGT and IGAIM methods (Fig. S13a–c and S14a–c in ESI†). In all the three methods, observed up-field chemical shift of the $O–CH_2$ protons was in agreement with the experimental observations. Thus, the close agreement between the theoretical and experimental spectra (UV-vis, IR and NMR) had strongly supported the optimized structure (Fig. 10).

### Cell imaging

Aluminum treated and untreated cells were incubated with the ligand and observed under a fluorescence microscope as described in the Experimental section. Fig. 12 indicates that the ligand is easily permeable to all types of living cells tested causing no harm (as cells remained alive even after 30 minutes of exposure to the ligand at 10 μM). Intensity of the fluorescence was almost the same after 15 minutes and 30 minutes (Fig. 12d and e).

## Conclusions

A facile synthesis of a naphthalene exciplex based water soluble $Al^{3+}$ chemosensor (**HL**) was described. Detection of $Al^{3+}$ by **HL** in living cells at physiological pH could be achieved. $Al^{3+}$ assisted fluorescence enhancement of **HL** was attributed to the absence of PET effect. The weak quenching effect of $Fe^{3+}$ and $Cu^{2+}$ on the fluorescence of **HL** did not hamper $Al^{3+}$ detection in living cells. Common metal ions and anions did not interfere. DFT and TDDFT studies have supported the experimental findings nicely. This new $Al^{3+}$ selective fluorescent probe may find potential biomedical applications. The present sensor has some merits over other existing sensors, *viz.* (i) less use of organic solvent, (ii) second highest detection limit (highest, ref. 13*a*), (iii) one step facile synthesis of the probe, (iv) least interference from other common ions, and (v) amongst few others who performed cell imaging studies. Moreover, Wang *et al.*[13a] have worked on human leukemia cells. It is well known that cancer cells show unusual properties than the normal cells.

## Acknowledgements

Authors sincerely thank West Bengal Council of Science and Technology and UGC-DAE-CRS-Kolkata for financial support. A. Sahana and S. Lohar are thankful to CSIR, New Delhi, for providing fellowship. We are thankful to Indian Institute of Chemical Biology (IICB), Kolkata, for extending the NMR and mass spectrometer facilities. We gratefully acknowledge the support of USIC (BU) for fluorescence microscope facility. We sincerely thank reviewers for constructive suggestions to enhance the quality of the article.

## References

1 M. Baral, S. K. Sahoo and B. K. Kanungo, *J. Inorg. Biochem.*, 2008, **102**, 1581.
2 M. Kawahara, K. Muramoto, K. Kobayashi, H. Mori and Y. Kroda, *Biochem. Biophys. Res. Commun.*, 1994, **198**, 531.
3 S. R. Paik, J. H. Lee, D. H. Kim, C. S. Chang and J. Kim, *Arch. Biochem. Biophys.*, 1997, **344**, 325.
4 J. L. Lin, M. T. Kou and M. L. Leu, *Nephron*, 1996, **74**, 33.
5 P. F. Good, C. W. Olanow and D. P. Perl, *Brain Res.*, 1992, **593**, 343.
6 R. A. Yokel, *Coord. Chem. Rev.*, 2002, **228**, 97.
7 G. R. Rout, S. Samanta Roy and P. Das, *Agronomie*, 2001, **21**, 3.
8 J. Halfield and B. A. Stewart, *Advances in Soil Sciences: Limitations to Plant Root Growth*, 1992, vol. 19, p. 97.
9 (*a*) J. Barcelo and C. Poschenrieder, *Environ. Exp. Bot.*, 2002, **48**, 75; (*b*) B. Valeur and I. Leray, *Coord. Chem. Rev.*, 2000, **205**, 3; (*c*) M. A. M. Rogers and D. G. Simon, *Age and Ageing*, 1999, **28**, 205; (*d*) Z. Krejpcio and R. W. Wojciak, *Pol. J. Environ. Stud.*, 2002, **11**, 251.
10 (*a*) T. Schraderr and A. D. Hamilton, *Functional Synthetic Receptors*, Wiley-VCH, Weinheim, Germany, 2005; (*b*) J. P. Desvergne, A. Czarnik and W. Kluwer, *Chemosensors of Ion and Molecule Recognition*, Dordrecht, 1997; (*c*) A. W. Czarnik, *Fluorescent Chemosensors for Ion and Molecule Recognition*, American Chemical Society, Washington, DC, 1992; (*d*) R. Martínez-Máñez and F. Sancenón, *Chem. Rev.*, 2003, **103**, 4419; (*e*) P. D. Beer and P. A. Gale, *Angew. Chem., Int. Ed.*, 2001, **40**, 486; (*f*) A. P. De Silva, H. Q. N. Gunaratne, T. Gunnlaugsson, A. J. M. Huxley, C. P. McCoy, J. T. Rademacher and T. E. Rice, *Chem. Rev.*, 1997, **97**, 1515.
11 (*a*) U. E. Spichiger-Keller, *Chemical Sensors and Biosensors for Medical and Biological Applications*, Wiley-VCH, Weinheim, Germany, 1998; (*b*) V. Amendola, L. Fabbrizzi, F. Forti, M. Licchelli, C. Mangano, P. Pallavicini, A. Poggi, D. Sacchi and A. Taglieti, *Coord. Chem. Rev.*, 2006, **250**, 273; (*c*) K. Rurack and U. Resch-Genger, *Chem. Soc. Rev.*, 2002, **31**, 116; (*d*) P. T. Srinivasan, T. Viraraghavan and K. S. Subramanian, *Water SA*, 1999, **25**, 47.
12 K. Soroka, R. S. Vithanage, D. A. Phillips, B. Walker and P. K. Dasgupta, *Anal. Chem.*, 1987, **59**, 629.
13 (*a*) L. Wang, W. Qin, X. Tang, W. Dou, W. Liu, Q. Teng and X. Yao, *Org. Biomol. Chem.*, 2010, **8**, 3751; (*b*) K. K. Upadhyay and A. Kumar, *Org. Biomol. Chem.*, 2010, **8**, 4892; (*c*) D. Maity and T. Govindaraju, *Chem. Commun.*, 2010, **46**, 4499; (*d*) M. Arduini, F. Felluga, F. Mancin, P. Rossi, P. Tecilla, U. Tonellato and N. Valentinuzzi, *Chem. Commun.*, 2003, 1606; (*e*) D. Maity and T. Govindaraju, *Inorg. Chem.*, 2010, **49**, 7229; (*f*) Y. W. Wang, M. X. Yu, Y. H. Yu, Z. P. Bai, Z. Shen, F. Y. Li and X. Z. You, *Tetrahedron Lett.*, 2009, **50**, 6169; (*g*) S. H. Kim, H. S. Choi, J. Kim, S. J. Lee, D. T. Quang and J. S. Kim, *Org. Lett.*, 2010, **12**, 560; (*h*) A. Sahana, A. Banerjee, S. Das, S. Lohar, D. Karak, B. Sarkar, S. K. Mukhopadhyay, A. K. Mukherjee and D. Das, *Org. Biomol. Chem.*, 2011, **9**, 552.

 

14 (*a*) N. Chattopadhyay, A. Mallick and S. Sengupta, *J. Photochem. Photobiol., A*, 2006, **177**, 55; (*b*) Y. G. Zhao, Z. H. Lin, H. P. Liao, C. Y. Duan and Q. J. Meng, *Inorg. Chem. Commun.*, 2006, **9**, 966.
15 D. P. Roek, J. E. Chateauneuf and J. F. Brennecke, *Ind. Eng. Chem. Res.*, 2000, **39**, 3090.
16 P. Frederick, S. P. Schwarz and K. Wasi, *Anal. Chem.*, 1976, **48**, 524.
17 M. Ali, M. Jha, S. K. Das and S. K. Saha, *J. Phys. Chem. B*, 2009, **113**, 15563.
18 M. J. Frisch, G. W. Trucks, H. B. Schlegel, G. E. Scuseria, M. A. Robb, J. R. Cheeseman, J. A. Montgomery, Jr., T. Vreven, K. N. Kudin, J. C. Burant, J. M. Millam, S. S. Iyengar, J. Tomasi, V. Barone, B. Mennucci, M. Cossi, G. Scalmani, N. Rega, G. A. Petersson, H. Nakatsuji, M. Hada, M. Ehara, K. Toyota, R. Fukuda, J. Hasegawa, M. Ishida, T. Nakajima, Y. Honda, O. Kitao, H. Nakai, M. Klene, X. Li, J. E. Knox, H. P. Hratchian, J. B. Cross, V. Bakken, C. Adamo, J. Jaramillo, R. Gomperts, R. E. Stratmann, O. Yazyev, A. J. Austin, R. Cammi, C. Pomelli, J. Ochterski, P. Y. Ayala, K. Morokuma, G. A. Voth, P. Salvador, J. J. Dannenberg, V. G. Zakrzewski, S. Dapprich, A. D. Daniels, M. C. Strain, O. Farkas, D. K. Malick, A. D. Rabuck, K. Raghavachari, J. B. Foresman, J. V. Ortiz, Q. Cui, A. G. Baboul, S. Clifford, J. Cioslowski, B. B. Stefanov, G. Liu, A. Liashenko, P. Piskorz, I. Komaromi, R. L. Martin, D. J. Fox, T. Keith, M. A. Al-Laham, C. Y. Peng, A. Nanayakkara, M. Challacombe, P. M. W. Gill, B. G. Johnson, W. Chen, M. W. Wong, C. Gonzalez and J. A. Pople, *GAUSSIAN 03 (Revision C.02)*, Gaussian, Inc., Wallingford, CT, 2004.
19 J. A. Ibemesi, M. Ashraf EL-Bayoumi and J. B. Kinsinger, *Chem. Phys. Lett.*, 1978, **53**, 270.
20 (*a*) S. Tal, H. Salman, Y. Abraham, M. Botoshanksy and Y. Eichen, *Chem.–Eur. J.*, 2006, **12**, 4858; (*b*) B. Ramachandram, G. Saroja, N. B. Sankaran and A. Samanta, *J. Phys. Chem. B*, 2000, **104**, 11824.
21 H. A. Benesi and J. H. Hildebrand, *J. Am. Chem. Soc.*, 1949, **71**, 2703.
22 (*a*) K. K. Upadhyay, A. Kumar, R. K. Mishra, T. M. Fyles, S. Upadhyay and K. Thapliyal, *New J. Chem.*, 2010, **34**, 1862; (*b*) K. K. Upadhyay and A. Kumar, *Talanta*, 2010, **82**, 845; (*c*) K. K. Upadhyay, R. K. Mishra, V. Kumar and P. K. Roy Chowdhury, *Talanta*, 2010, **82**, 312; (*d*) K. K. Upadhyay, A. Kumar, J. Zhao and R. K. Mishra, *Talanta*, 2010, **81**, 714; (*e*) Y. Zhao, Z. Lin, H. Liao, C. Duan and Q. Meng, *Inorg. Chem. Commun.*, 2006, **9**, 966; (*f*) F. Hueso, N. A. Illán, M. N. Moreno, J. M. Martínez and M. J. Ramírez, *J. Inorg. Biochem.*, 2003, **94**, 326; (*g*) Y. Zhou, H. N. Kim and J. Yoon, *Bioorg. Med. Chem. Lett.*, 2010, **20**, 125.
23 (*a*) S. Miertus, E. Scrocco and J. Tomasi, *Chem. Phys.*, 1981, **55**, 117; (*b*) M. Cossi, V. Barone, R. Cammi and J. Tomasi, *Chem. Phys. Lett.*, 1996, **255**, 327; (*c*) M. Cossi, V. Barone and M. A. J. Robb, *Chem. Phys.*, 1999, **111**, 5295; (*d*) M. Cossi, G. Scalmani, N. Rega and V. J. Barone, *Chem. Phys.*, 2002, **117**, 43.